Paper:

Extraction of Inundation Areas Due to the July 2018 Western Japan Torrential Rain Event Using Multi-Temporal ALOS-2 Images

Wen Liu†, Fumio Yamazaki, and Yoshihisa Maruyama

Graduate School of Engineering, Chiba University
1-33 Yayoi-cho, Inage-ku, Chiba 263-8522, Japan
†Corresponding author, E-mail: wen.liu@chiba-u.jp
[Received November 12, 2018; accepted February 22, 2019]

A series of heavy rainfalls hit the western half of Japan from June 28 to July 8, 2018. Increased river water overflowed and destroyed river banks, causing flooding over vast areas. In this study, two pre-event and one co-event ALOS-2 PALSAR-2 images were used to extract inundation areas in Kurashiki and Okayama Cities, Okayama Prefecture, Japan. First, water regions were extracted by threshold values from three-temporal intensity images. The increased water regions in July 2018 were obtained as inundation. Inundated built-up areas were identified by the increase of backscattering intensity. Differences between the pre- and co-event coherence values were calculated. The area with decreased coherence was extracted as a possible inundation area. The results of a field survey conducted on July 16, 2018 were used to estimate the optimal parameters for the extraction. Finally, the results from the intensity and coherence images were verified by making comparisons between a web-based questionnaire survey report and the visual interpretation of aerial photographs.

Keywords: ALOS-2 PALSAR-2, backscattering intensity, coherence, land-cover map, flood

1. Introduction

Due to a stationary seasonal Baiu rain front and the typhoon Prapiroon, (Typhoon Number 7) from June 28 to July 8, 2018, multiple rounds of heavy rainfall occurred in Kyushu, Shikoku, and the western Honshu regions of Japan (**Fig. 1**) [1]. Half of the Japanese territory received heavy rainfall of more than 500 mm. The Japan Meteorological Agency (JMA) issued emergency heavy rain warnings in eleven prefectures, which was the highest level of warning issued since its implementation. Increased water levels in rivers caused overflows and bank failures. By October 9, 2018, 2,512 landslides were reported from 31 prefectures [2]. Due to these inundations and landslides, 224 people were killed, 8 were missing, 6,695 buildings had collapsed or were severely damaged,

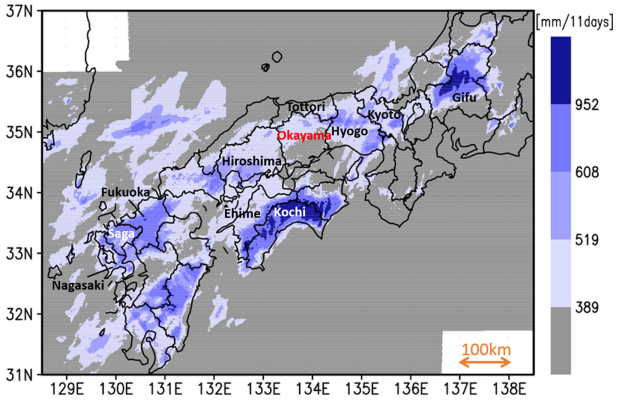

Fig. 1. Cumulative rainfall from June 28 0:00 to July 8 24:00 (JST), 2018 [1]. The eleven prefectures with issued warnings are indicated on the map.

and approximately 30,000 were flooded.

Remote sensing is useful for determining broad-scale damage situations. Synthetic aperture radar (SAR) sensors are more powerful than optical sensors to extract flooded areas after heavy rainfall events because SAR can make day- and night-time observations, even under cloud-cover conditions. According to the law of specular reflection, most incident radar energy impinging on mirror-like smooth water surfaces, reflect in the opposite direction. Water regions in a SAR image show low backscattering intensity and as such, SAR images are effective for identifying inundations. Both pixel-based and object-based methods have been proposed to extract inundated zones from SAR images [3–9]. The flooded area could be extracted by thresholding methods using the gray-level histogram either manually or with automation [8–10]. However, the thresholding of the backscattering intensity was difficult to apply for built-up areas containing layover and radar shadow [11]. To overcome this problem, the image differencing method and SAR simulation using Lidar data were proposed [11–13]. Interferometric coherence has been shown to be valid for identifying inundated urban areas [14–16]. However, its applicability is limited by the strict requirement of temporal and spatial baselines and the lack of archive data.

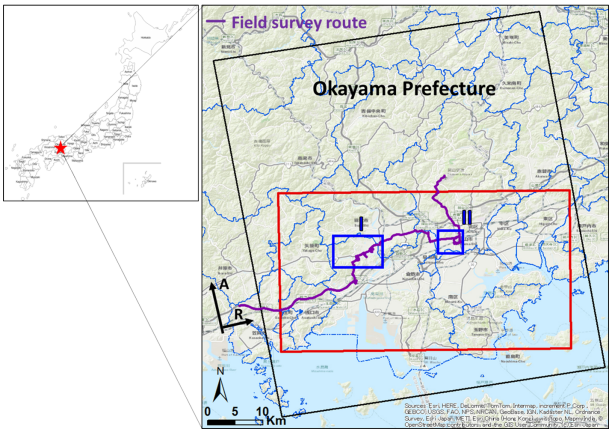

Fig. 2. Coverage of the ALOS-2 images (black frame) and the target area (red square). Purple line indicates the field survey route on July 16, 2018. The red frame is the target area including Kurashiki City and a part of Okayama City.

When comparing with L-band SAR images, X-and C-band images with short wavelengths and higher resolutions were used more widely in flood mapping. A follow-up satellite of the ALOS program is ALOS-2, which was launched on 24 May 2014. It carries the PALSAR-2 enhanced high-resolution L-band SAR sensor. Owing to the right- and left-looking function of the PALSAR-2 sensor, emergency observations are possible in a short time period. PALSAR-2 images have been used to extract inundation areas from several flood events around the world [6, 9, 11, 17, 18].

In this study, we attempted to identify inundated areas in Kurashiki and Okayama Cities in the Okayama Prefecture using pre-and co-event PALSAR-2 images. The inundations were extracted using backscattering intensity and coherence values. In addition, a field survey was carried out to confirm the results from the PALSAR-2 images. Finally, the accuracy of the flood extraction was verified by introducing a web-based questionnaire survey report and other references. Instead of proposing a new method, we applied the known methods to this new event to discuss the optimal threshold values and their applicability.

2. Study Area and Field Survey

The study area was the Okayama Prefecture, one of the areas worst affected by the heavy rain event. Eleven out of 25 observation points of the Automated Meteorological Data Acquisition System (AMeDAS) recorded more than 400 mm cumulative precipitation from July 3 to July 8 [19] (**Fig. 2**). The maximum 24-hour cumulative precipitation was 138.5 mm in Kurashiki City and 165.0 mm in Kita-ku, Okayama City.

A heavy rain warning was issued for Kurashiki City at 18:30 (JST) on July 5. The flood warnings for Takahashi and Oda Rivers were issued sequentially between 20:00 and 22:20 on July 6, and an evacuation advisory was issued for the entire Mabi town at 22:00 on July 6. Early on July 7, three overflows and eight bank failures occurred, which caused a 12-km^2 area of inundation in Mabi town. The longest bank failure was on the left side of Oda River and was approximately 200 m in length. Fifty-one people were killed by the floodwater and 4,600 buildings were inundated [20].

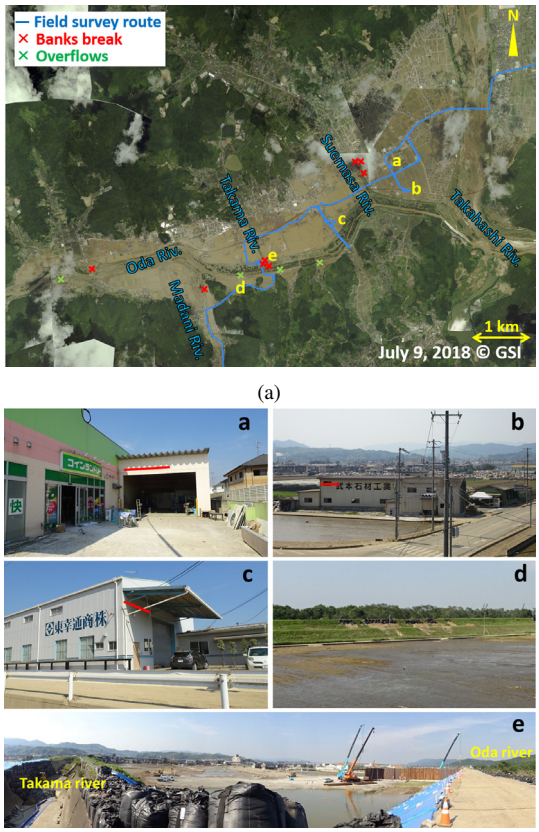

Fig. 3. (a) Mosaicked aerial photo of Mabi town, Kurashiki City (I), taken by GSI on July 9, 2018 [21]. Locations of bank failures and overflows are marked by the cross symbols. (b) Ground photos taken in the field survey on July 16, 2018, at the locations **a**–**e** in (a).

The heavy rain warning was issued for Okayama City at 15:39 on July 5, and flood warnings for Sasagase and Ashimori Rivers were issued at 15:30 on July 6. The flood warning for Asahi River was issued at 23:35 on July 6. A 120-m bank failure of Sunagawa River, a tributary of the Asahi river system, was observed at approximately 5:30 on July 7. It flooded a 7.5-km^2 area in Higashi-ku. Furthermore, a 50-m bank failure of Asahi River was confirmed on July 7, which caused inundation in Kitsukunigahara, Kita-ku. Due to these failures, more than 2,000 buildings were flooded in Okayama City.

We conducted a field survey in Okayama Prefecture on July 16, 2018 (**Fig. 2**). We investigated the inundation conditions in Mabi town, Kurashiki City (I) and Kume, Kita-ku, Okayama City (II) in detail. **Fig. 3(a)** shows a mosaicked aerial photograph taken over Mabi town by the Geospatial Information Authority of Japan (GSI) on

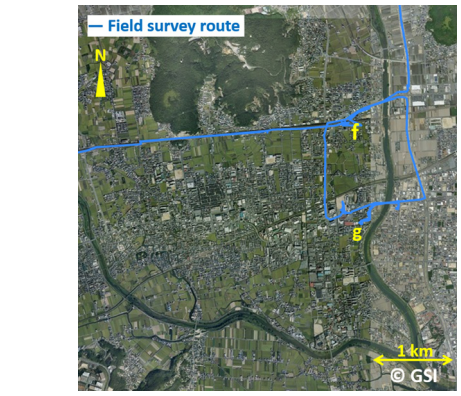

(a)

(b)

Fig. 4. (a) Mosaicked aerial photo of Kume, Kita-ku, Okayama City (II), taken by GSI before the event [21]. (b) Ground photos from the field survey on July 16, 2018, at the locations **f**–**g** in (a).

July 9, 2018 [21]. Although it was taken two days after the flood event, extensive inundations could still be confirmed at the center of Mabi town from the aerial photograph. Two bank failures and three overflows occurred in Oda River whereas the other six bank failures occurred in its tributaries.

At the inspection of Mabi town one week after the event, most of the inundations had dried up. Five ground photographs taken at the locations **a** to **e** are shown in **Fig. 3(b)**. The photograph **a** shows a supermarket, where the inundation was over the ceiling of the ground floor. However, it had re-opened when the site was visited. A watermark remained on the wall, 3.9 m from ground level and is indicated by a red line in the photograph. The photographs **b** and **c** show a factory building and a warehouse, respectively. Watermarks can be observed on the wall and both are higher than 4 m. The photograph **d** was taken at one of the overflows. Water remained in inundated agriculture fields. Many sandbags for emergency restoration of the bank can be seen in the ground photograph. The location **e** is the junction of Oda River and its tributary Takama River. Three bank failures occurred at this location. The length of the collapsed bank of Oda River was 200 m. The temporary banks of the Oda and Takama rivers, which were built using concrete blocks and sandbags, can be seen in the panoramic photograph **e**.

There was little news regarding the flood situation in Kume, Kita-ku in Okayama City. Thus, the GSI did not take any aerial photographs of this area after the rainfall event. A pre-event aerial photograph is shown in **Fig. 4(a)**. Since many waterways cross the residential blocks, this area was flooded due to the increase of water in the Sasagase river system. Two ground photographs taken at the locations **f** and **g** are shown in **Fig. 4(b)**. The location **f** is near the Sanyo Shinkansen railway. No obvious watermark was observed during the field survey. However, information from residents revealed that an inundation of approximately 50 cm above the road level occurred during the rainfall event. The photograph **g** shows a watermark remaining on a building wall, about 50 cm from ground level. Local people produced several photographs taken during the flood where the water was above the ground floor.

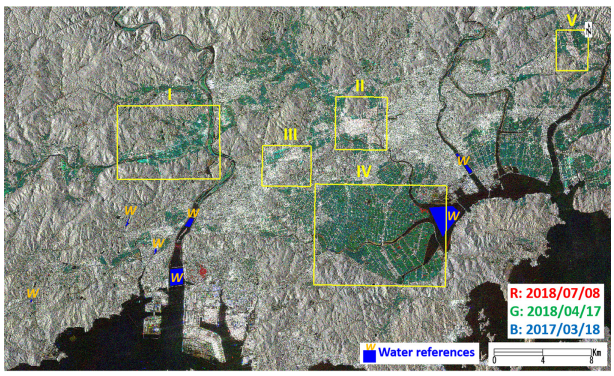

Fig. 5. Color composite of the pre-and co-event PALSAR-2 sigma naught images.

3. Image Data and Pre-Processing

ALOS-2 made an emergency observation in the descending path at 00:05 on July 8, 2018, 24 hours after the bank failures. The coverage of the ALOS-2 observation is indicated in **Fig. 2** by the black frame. In the same path, two most recent archive data were taken on March 18, 2017 and on April 17, 2018. These images were acquired in the StripMap-1 mode with a 3-m spatial resolution by HH polarization. The original images were Single Look Complex (SLC) data in processing Level 1.1. After registration and multi-look (2 looks in each direction) processing, the amplitude images were geocoded by a 5 m digital elevation model of GSI [22] with a spacing of 2.5 m/pixel. The backscattering intensities (sigma naught values σ^0) were obtained after radiometric calibration [23]. The pre-processing steps were carried out using ENVI SARscape software. To retain the resolution, a speckle filter was not applied.

The color composite of the two pre-event and one co-event images after the pre-processing is shown in **Fig. 5**. Since the two pre-event images were taken in the same season, the backscatter values in these images were similar, showing cyan color in the color composite. Thus, the cyan areas in **Fig. 5** represent the decrease of backscatter in the co-event image.

A 10-m land-cover map was introduced to assist with the interpretation of the land-cover situation of the target area. The land-cover map was produced using multi-

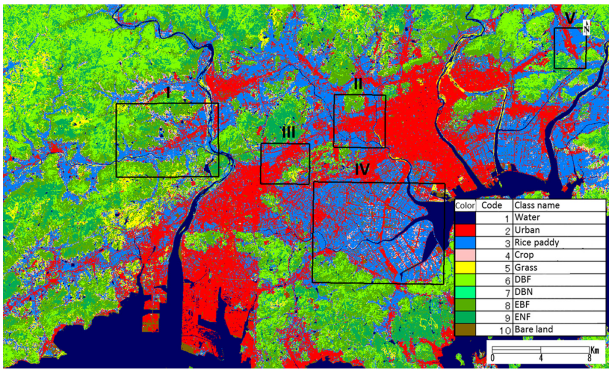

Fig. 6. Land-cover map produced by JAXA from multi-temporal AVNIR-2 optical satellite data [24, 25].

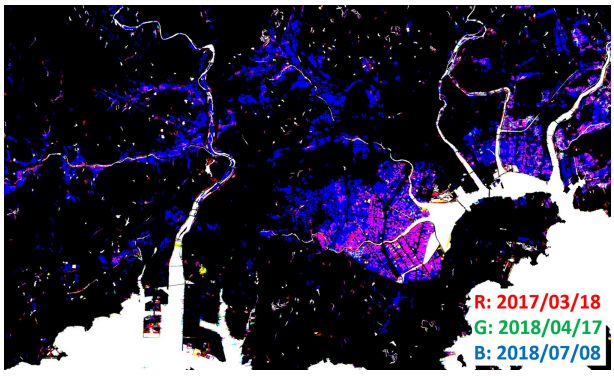

Fig. 7. Color composite of water regions extracted by the threshold of backscattering intensity for each image.

temporal ALOS AVNIR-2 data [24] and published digitally by JAXA [25]. The land covers were classified into 10 classes: water, urban, rice paddy, crop, grass, deciduous broad-leaved forest (DBF), deciduous needle-leaved forest (DNF), evergreen broad-leaved forest (EBF), evergreen needle-leaved forest (ENF), and bare land (**Fig. 6**).

In addition to the two areas visited in the field survey (I and II), three other areas are indicated by yellow squares (**Fig. 5**). Area III is Nakasho, Kurashiki City, and is primarily urbanized land. Due to the flood of Rokken River, one of the tributaries of Kurashiki River inundated several roads in the Nakasho area. However, the decrease of backscattering was only seen in the rice paddy field. The area IV in **Fig. 6** denotes agriculture lands in Minami-ku, Okayama City, which shows cyan color widely in **Fig. 5**. The area V is Hirajima, Higashi-ku in Okayama City. A bank failure in Sunagawa River caused the second largest inundation in Okayama Prefecture in this area. The decrease of backscatter can be observed from the rice paddy fields in **Fig. 5**, but there were no significant changes in the built-up area.

4. Extraction of Inundation Using Backscattering Intensity

Thresholding is a common and effective pixel-based approach to extract water bodies from SAR intensity images [8–10]. The backscattering of a water surface depends on many factors such as acquisition conditions of SAR images and their environments, and therefore its value is highly variable. In the previous study [9], a comparison of the threshold values obtained by the optimal solution and by the statistical features (mean and standard deviation) was carried out using water and non-water references. As a result, the combinations using the mean (μ) and standard deviation (σ) values ($\mu+2\sigma$) of the water references were close to the optimal threshold values. Thus, the same method was applied in this study.

Seven water references over a total area of 5.5 km^2 were selected from the SAR intensity images. Their locations are indicated in **Fig. 5** by blue polygons. Three of these are reservoirs in Kurashiki City, and others are parts of Takahashi River and Kojima Lake. The threshold values were calculated using the mean value plus two standard deviations, $\mu+2\sigma$, of the water references. Since the three images were taken in the same acquisition condition, the obtained threshold values of $\mu+2\sigma$ were similar; -12.8 dB on March 18, 2017, -12.3 dB on April 17 and -12.0 dB on July 8, 2018, respectively.

From the PALSAR-2 image on March 18, 2017, a total area of 276 m^2 was extracted as water. In the land-cover map, a total water surface of 236 m^2 exists in the target area, and 78% (producer accuracy) was extracted successfully. The precision (user accuracy) was 92%, and the F1 score of the water extraction was 0.84. The F1 score is a harmonic average of the precision (user accuracy) and recall (producer accuracy), where it reaches its best value at 1 and worst value at 0 [26]. In the extracted area, the rice paddy fields occupied a total area of 12%. In March, the dry rice paddies were as smooth as bare land. Due to the long wavelength of L-band, those areas were incorrectly extracted as water regions. From the PALSAR-2 image on April 17, 2018, a 236-m^2 area was extracted as water, corresponding to the 91% water in the land-cover map. The precision was also 91%. The F1 score of the water extraction was 0.91. Only 3% of the extracted area was rice paddy fields. The decrease in the extracted rice paddy was due to the rough surface after tillage work occurred in April. According to these comparisons, the threshold values obtained from the mean and standard deviation values of the water references were verified as valid. Using the threshold value of -12.0 dB, a total area of 382 km^2 was then extracted as water from the PALSAR-2 image on July 8, 2018. The rice paddies occupied 32%. According to Ouchi et al. [27], the backscatter intensity of rice paddies is very low in this season. Thus, the no-flood rice paddies would also be extracted by the proposed thresholding method.

The color composite of the extracted water regions is shown in **Fig. 7**. The existing water regions in the land-cover map were masked in the result. When comparing to the land-cover map, aside from the additional water regions shown in blue colors, the water regions extracted

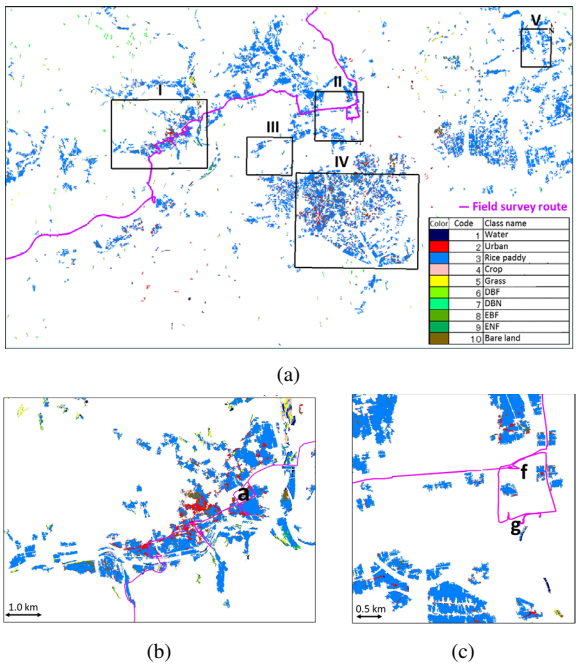

(a) (b) (c)

Fig. 8. (a) Additional water regions in the co-event image after removing the pre-event water surfaces. Colors indicate land covers by JAXA, with (b)–(c) close-up of the areas I and II.

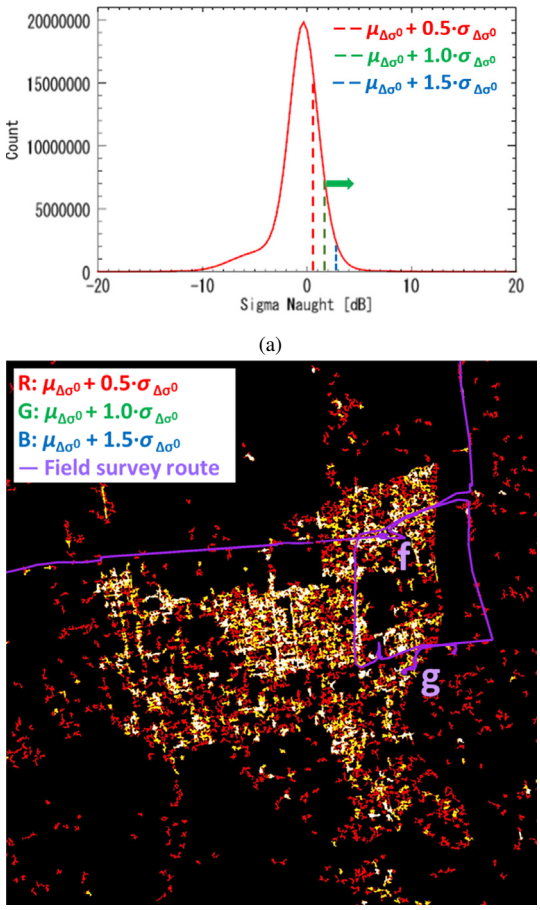

(a) (b)

Fig. 9. (a) Histogram of the difference of the sigma naught values of the SAR images on April 17 and July 8, 2018. (b) Comparison of the extracted built-up areas using the different combinations of the mean and standard deviation values of $\Delta\sigma^0$.

on March 18, 2017 (magenta colors) are primarily rice paddies. We masked the pre-event water regions from the co-event regions to detect additional water regions. The non-water area was less than 0.01 km^2 and if surrounded by water were re-classified into water regions. The water region smaller than 0.01 km^2 was removed from the water class as noise. Finally, a total area of 106 km^2 was extracted as inundation, which consisted of 83% rice paddy fields, 7% urban areas and 4% bare lands (**Fig. 8(a)**).

The enlarged areas I and II are shown in **Figs. 8(b)** and **(c)**. Vast inundation was extracted in Mabi town, Kurashiki City (I). However, the location **a** was excluded from the result. The buildings of the supermarket are higher than the flood water level, and therefore the double-bounce between the left wall and the water surface showed strong backscatter [7, 12, 13, 18]. When a building has been completely inundated, its reflection decreases as water surface. However, the backscatter increases when a building is partially inundated. Thus, the partially inundated built-up area could not be extracted by the proposed method. The same problem occurred in area II. The locations **f** and **g** were out of the extracted inundation (**Fig. 8(c)**).

To detect the flooded urban area, the backscatter intensity difference between the PALSAR-2 images on April 17 and July 8, 2018 was calculated. The built-up area with increased backscatter intensity was identified as inundation [7, 9]. A histogram of the difference $\Delta\sigma^0$ (co-event–pre-event) in the entire target area is shown in **Fig. 9(a)**. Three threshold values were investigated using the combinations of the mean ($\mu_{\Delta\sigma^0}$) and the standard deviation ($\sigma_{\Delta\sigma^0}$). The mean value of the whole target area was -0.6 dB with the standard deviation 2.3 dB. In the previous study [9], the threshold was set as $\mu_{\Delta\sigma^0} + 2.0\sigma_{\Delta\sigma^0}$ for the extraction. However, this threshold was strict for this event. The comparison of results using the different threshold values in the area II is shown in **Fig. 9(b)**. When the threshold value was set as 2.88 dB ($\mu_{\Delta\sigma^0} + 1.5\sigma_{\Delta\sigma^0}$), the extracted regions were shown in white (**Fig. 9(b)**). The locations **f** and **g** were still excluded from the extraction. When the threshold value was set as 0.56 dB ($\mu_{\Delta\sigma^0} + 0.5\sigma_{\Delta\sigma^0}$), the locations **f** and **g** could be extracted, but the result included a lot of noise (red regions). Since the threshold value of 1.72 dB ($\mu_{\Delta\sigma^0} + 1.0\sigma_{\Delta\sigma^0}$) could estimate the inundation at the locations **f** and **g** with less noise, this value was adopted to estimate the flooded urban area (yellow regions). The difference between the best optimal threshold values for the different events may be caused by different inundation depths. The inundation was deeper than 80 cm in the previous event, whereas it was approximately 50 cm in area II of this event.

The inundation map was modified by adding the flooded urban areas (**Fig. 10**). The inundated built-up pix-

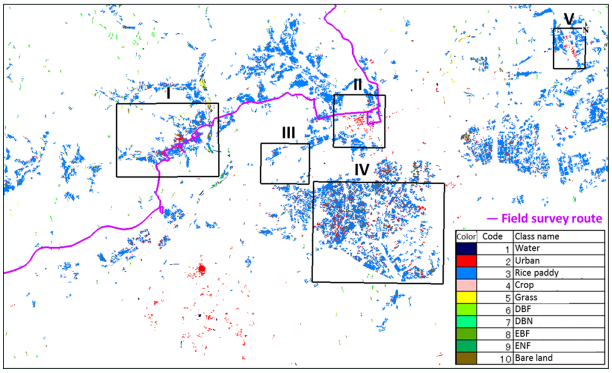

Fig. 10. Modified result by adding the inundated urban areas extracted by the increase of the backscatter intensity.

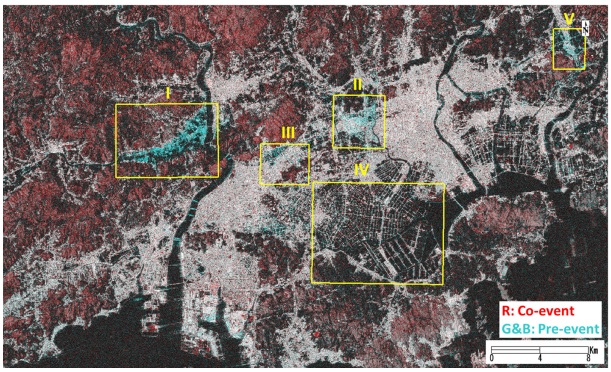

Fig. 11. Color composite of the pre- and co-event coherence values of the three temporal PALSAR-2 data.

els in the area V that could not be detected in the previous step were included in the new result. The extracted inundation area increased to 108 km^2, including 81% rice paddy fields, 9% urban land-covers and 4% bare lands. However, the inundated urban area in Mabi town (I) remained unable to be estimated. Although the multiple reflections from buildings and water surfaces still occurred in Mabi town, deep inundation reduced the backscattering intensity. Thus, it is difficult to extract flooded areas using increased backscatter.

5. Extraction of Inundation Using Interferometric Coherence

The pre- and co-event coherences were calculated from the three temporal PALSAR-2 complex data. The image on April 17, 2018 was set as the master, and the other two images were set as slaves. The color composite of the pre- and co-event coherences is shown in **Fig. 11**. Similar to the colors in **Fig. 5**, the cyan areas represent the decrease of coherence after the flood event.

The coherence in an urban area was high and stable, as indicated in white in **Fig. 11**. As the temporal baseline of the co-event coherence (4 months) was shorter than that of the pre-event pair (one year), the co-event coherence

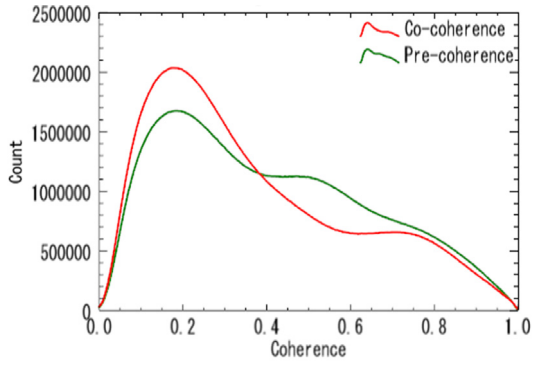

(a)

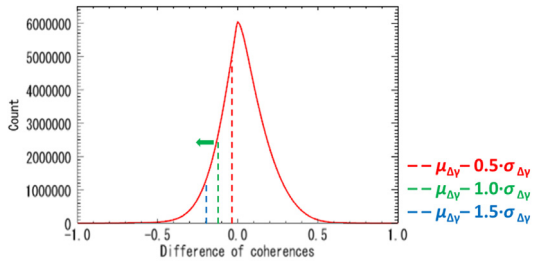

(b)

Fig. 12. (a) Histograms of the pre- and co-event coherences; (b) histogram of the difference between the pre- and co-event coherences.

values in vegetated areas (grass and forest) were mostly higher than the pre-event values and thus are seen in red (**Fig. 11**). Due to the different roughness of rice paddy fields in March (smooth), April (a little rough) and July (smooth), the pre- and co-event coherences were both low. In area I of Mabi town, a decrease in coherence can be observed widely, as in **Fig. 11**. The built-up areas II, III and V display more cyan-colored areas colors in **Fig. 11**, which indicates possible flooding.

The area IV shows low values in both the pre- and co-event coherences. Since no significant decrease of coherence can be seen in this area, and the roads between agriculture fields show high coherence values, the possibility of flooding in this area is low. The decreasing backscattering intensity shown in **Fig. 5** is considered to be caused by irrigation of the rice paddy fields after the acquisition of the image dating April 17, 2018.

The histograms of the pre- and co-event coherences are shown in **Fig. 12**. The decreased portion in the co-event coherence was considered to be inundation. The differences $\Delta\gamma$ were calculated by subtracting the pre-event value from the co-event value. The mean of difference ($\mu_{\Delta\gamma}$) in the entire study area was 0.04, and the standard deviation ($\sigma_{\Delta\gamma}$) was 0.16. When the threshold value was set as -0.20, meaning $\mu_{\Delta\gamma}-1.5\sigma_{\Delta\gamma}$, the extracted regions are displayed in white (**Fig. 13**). The location **d** in area I, which was flooded due to the overflows, and the location **g** in the area II could not be detected. When the threshold value was set as -0.04, meaning $\mu_{\Delta\gamma}-0.5\sigma_{\Delta\gamma}$, both the locations **d** and **g** could be detected, but the result included a large amount of noise, displayed in red (**Fig. 13**).

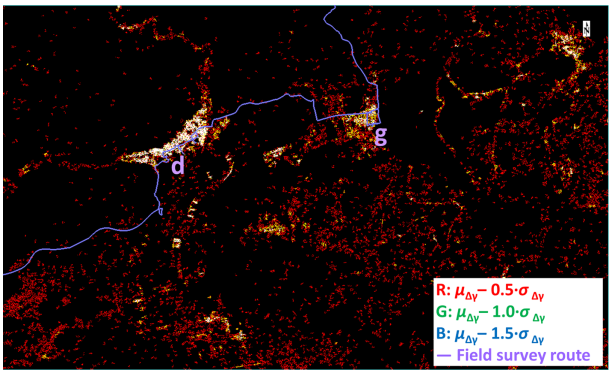

Fig. 13. Comparison of the extracted inundation using the different combinations of the mean and standard deviation values of $\Delta\gamma$.

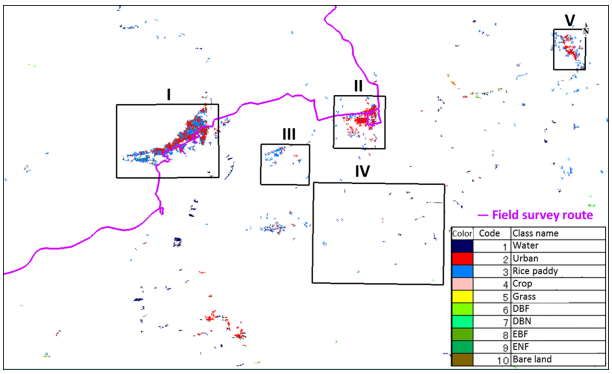

Fig. 14. Extracted inundation areas using the difference of the preand co-event coherence values.

Thus, the threshold value -0.12, which corresponds to $\mu_{\Delta\gamma} - 1.0\sigma_{\Delta\gamma}$, was adopted for the extraction, where the locations **d** and **g** could be detected with less noise.

The areas with a coherence difference lower than -0.12 were extracted as inundation. The hole-filling and noise-reducing processes were also applied to the areas smaller than 0.01 km^2. A total area of 19 km^2 was extracted as inundation, including 40% rice paddy fields, 35% urban land-covers and 11% water. The land covers of the inundation areas are shown in **Fig. 14** and primarily consisted of urban land use and some rice paddy fields. The extracted water land covers were the locations of bridges over Takahashi River. Due to an increased water level in Takahashi River, the pattern of the multiple reflections between the bridges and the water changed, which decreased coherence. Wide inundations were detected in areas I, II, and V, whereas little inundation was extracted in areas III and IV. Compared with the results shown in **Fig. 10**, the extracted urban area increased, and the rice paddy fields decreased significantly.

6. Verification of The Extraction Results

Our results extracted from the backscattering intensity and coherence were verified by comparing them with a map of the maximum inundation depth (**Fig. 15**). The inundation map was created according to an emergency questionnaire survey by Weathernews Inc. [28] on July 7, 2018. The inundation depths were classified into 4 levels: above waist (purple), above knee (red), above ankle (yellow) and a large puddle (blue). The extracted inundations matched the locations of the purple (above waist) and red (above knee) points. The results of matching the inundation locations reported by the emergency questionnaire survey to the extracted inundations are shown in **Table 1**. Due to the low location accuracy of the inundation points, if they were located within 100 m of the extracted inundation results, they were counted as matched points. Thirty-one percent of the purple and red (above waist and knee) points were included in the inundation that was extracted using the intensity images, whereas 29% were included in the results using the coherence images. Omission errors were derived from the difference between the SAR image acquisition time and the time of maximum water level. The commission errors (the yellow and green points within the extracted inundations) comprised 75% of the result using the intensity images and 44% using the coherence images. The results of the emergency questionnaire survey were biased, depending upon the degree of damage. For example, people in the severely damaged areas did not answer the survey, with only one point reported in Mabi town (I) and two points reported in the inundated Higashi-ku (V). Furthermore, coordinates of the inundation points were assigned automatically when participants answered the survey, and because the respondents would not answer the survey when they were in an inundation situation above knee or waist, their points were not matched to their real locations. This is one possible reason for the omission errors.

Zoomed in images of areas I and II are shown in **Fig. 16**. In area I (Mabi town), only one person reported an above-waist inundation depth. The central part of Mabi town was severely flooded from early July 7 and therefore the residents were forced to evacuate and could not answer the survey. The one reported point falls in the area extracted from the coherence difference. In area II, one point of the water depth higher than waist and eight points higher than knee were reported. The eight points higher than knee are located on or close to our extracted inundations from both the intensity and the coherence images. Furthermore, eight points higher than ankle overlapped on either the intensity or the coherence results. However, the inundated points in area III could not be extracted by our results. There was little change in this area in both the intensity and coherence images. When limited by a lack of information, it is difficult to determine the reason. In area IV, no inundation was reported by the survey, which matched the result obtained from the coherence difference. In area V, one point was reported as a water depth of higher than knee (red point), while considerable inun-

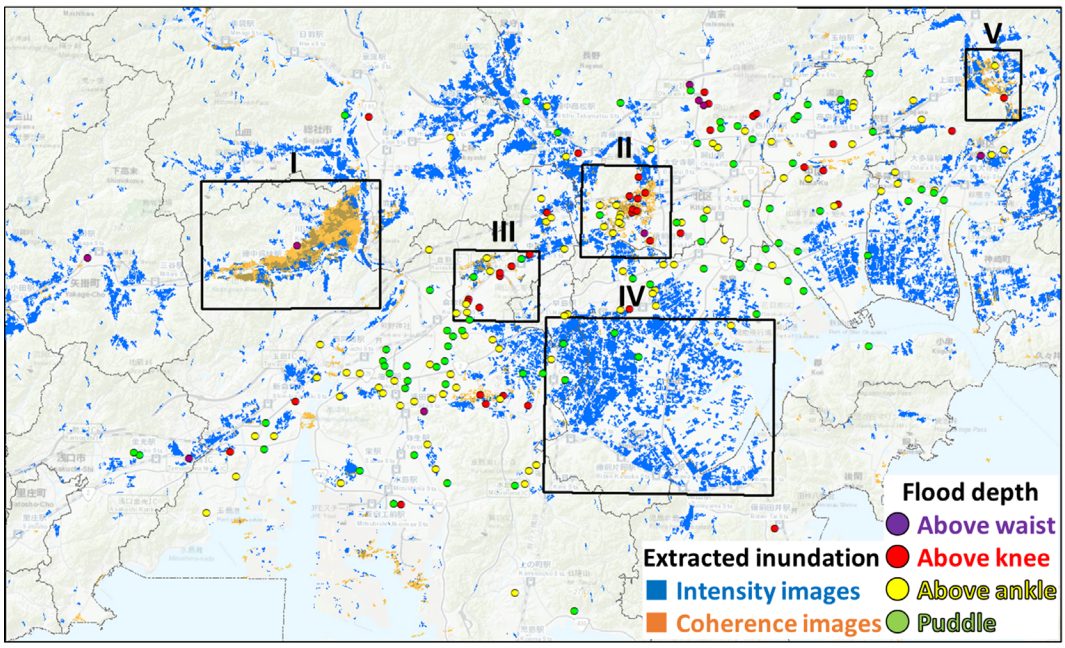

Fig. 15. Comparison of the extracted inundation using the intensity and coherence images, with an inundation map of emergency questionnaire survey by Weathernews Inc. [28]. The result from the intensity images is shown by the blue polygons and from the coherence images by the yellow polygons. The inundation depths reported by the questionnaire survey are indicated by points.

Table 1. Comparison of the inundated locations extracted from the PALSAR-2 images and reported by Weathernews Inc. [27].

		Weathernews Inc.				Total
		Above waist	Above knee	Above ankle	Puddles	
Extracted inundations	Intensity images	1	15	32	17	65
	Coherence images	2	13	11	1	27
Total		10	41	87	41	222

dation was extracted by the coherence difference.

According to the comparisons, our method appears to be effective in detecting an inundation of higher than 50 cm. Extraction using the coherence difference showed higher accuracy than when using the backscattering intensity. The backscatter intensity of agricultural fields was significantly influenced by seasons. Many rice paddy fields were extracted incorrectly in this study. Additional information is necessary to remove these errors. Although the intensity difference could extract parts of the inundated urban areas, its sensitivity was less than the coherence difference.

The Geospatial Information Authority of Japan (GSI) published daily inundation maps from July 7 to 11, 2018 [29]. The inundation on July 7 was estimated according to the DEM by adding several flooding points confirmed from videos, with a total area of 8.8 km^2. The outline of the inundation boundary on July 7 is shown in **Fig. 16(a)**. When comparing this with the GSI's result, 54% of the inundation in this area could be detected from the PALSAR-2 intensity images. The precision was 63%, and the F1 score was 0.58. Using the coherence difference, 72% of the inundated area could be extracted. The precision was 85%, and the F1 score was 0.78. The accuracies of the extraction using the coherence difference were higher than when using the backscattering intensity. The combination of the two results was considered.

7. Conclusions

In this study, the inundation areas in Kurashiki and Okayama Cities, Okayama Prefecture, Japan, resulting from the July 2018 western Japan torrential rain were extracted using two pre-event and one co-event ALOS-2 PALSAR-2 image. The water regions in the three temporal SAR intensity images were extracted by the respective threshold value of the backscattering intensity. The additional water regions on July 8, 2018 were obtained by removing the water regions in the pre-event images. 83% of the extracted area was comprised of rice paddy fields. The inundated urban area was extracted by the threshold value of the intensity difference between the SAR images on April 17 and July 8, 2018. As a result, 108 km^2 of

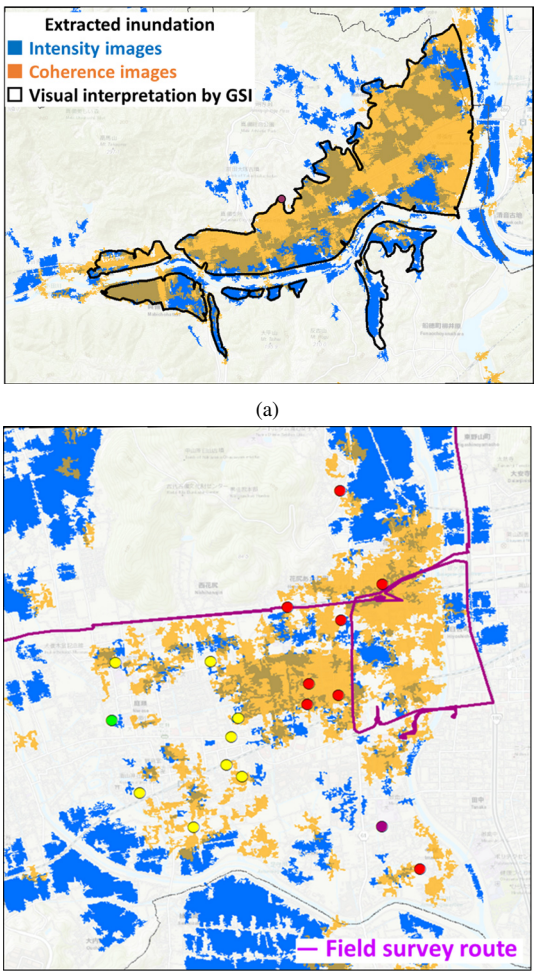

Fig. 16. (a) Zoomed in image of area I in Mabi town, Kurashiki City, with an inundation outline produced by GSI [29]. (b) Zoomed in image of area II in Kume, Kita-ku, Okayama City.

inundation were detected from the 1500-km^2 target area.

The difference between the pre-event and co-event coherence values was then calculated. By thresholding the difference using a combination of the mean and standard deviation, a total area of 19 km^2 of inundation was extracted. Although the extracted areas were less than those extracted from the intensity images, the inundation in both the urban land use and the rice paddies were extracted successfully.

A field survey of Mabi town, Kirashiki City and Kume, Kita-ku, Okayama City was carried out on July 16, 2018. The flooded locations found by observation and residents' interviews were used as references to determine the optimal threshold values for flood extraction. A map of the maximum inundation depth reported by a questionnaire survey of Weathernews Inc. was used to verify our results. The extracted inundation from both the intensity and the coherence images showed good agreement with the map of the water depth higher than knee. However, the extraction using coherence was better than that using intensity. Verification was also conducted by a comparison with the visual interpretation map by GSI for Mabi town. The two results from the coherence images showed the better F-score value as 0.78. In the future, inundation depth will be estimated by applying our results to a high-resolution DEM.

Acknowledgements

The ALOS-2 PALSAR-2 data used in this study are owned by the Japan Aerospace Exploration Agency (JAXA) and were provided for the ALOS-2 research program (RA6, PI No.3243). This work was partially supported by JST CREST (Grant Number JPMJCR1411), Japan, and JSPS KAKENHI (Grant Number 17H02066), Japan.

References:

[1] National Research Institute of Earth Science and Disaster Resilience (NIED), Storm, Flood and Landslide Reseach Division, "The characteristics of accumulated rainfall of the July 2018 Western Japan torrential rain," 2018, http://mizu.bosai.go.jp/key/RainJulyH30Accu (in Japanese) [accessed November 6, 2018]

[2] Cabinet Office, Government of Japan, Disaster Mangement, "Damage situation due to the July 2018 Western Japan torrential rain," 2018, http://www.bousai.go.jp/updates/h30typhoon7/pdf/301009_1700_h30typhoon7_01.pdf (in Japanese) [accessed November 6, 2018]

[3] S. Martinis, A. Twele, and S. Voigt, "Towards operational near-real time flood detection using a split-based automatic thresholding procedure on high resolution TerraSAR-X data," Natural Hazards and Earth System Sciences, Vol.9, pp. 303-314, doi: 10.5194/nhess-9-303-2009, 2009.

[4] S. Martinis, A. Twele, and S. Voigt, "Unsupervised extraction of flood-induced backscatter changes in SAR data using Markov image modeling on irregular graphs," IEEE Trans. on Geoscience and Remote Sensing, Vol.49, No.1, pp. 251-263, doi: 10.1109/TGRS.2010.2052816, 2011.

[5] L. Pulvirenti, N. Pierdicca, G. Boni, M. Fiorini, and R. Rudari, "Flood damage assessment through multitemporal COSMO-SkyMed data and hydrodynamic models: The Albania 2010 case study," IEEE J. of Selected Topics in Applied Earth Observations and Remote Sensing, Vol.7, pp. 2848-2855, doi: 10.1109/JSTARS.2014.2328012, 2014.

[6] F. Yulianto, P. Sofan, A. Zubaidah, K. A. D. Sukowati, and J. M. Pasaribu, "Detecting areas affected by flood using multitemporal ALOS PALSAR remotely sensed data in Karawang, West Java, Indonesia," Natural Hazards, Vol.77, No.2, pp. 959-985, doi: 10.1007/s11069-015-1633-x, 2015.

[7] M. Arri, "Sensitivity study of ALOS-2 data to floodwaters in Joso City in 2015 and its application," J. of The Remote Sensing Society of Japan, Vol.38, No.4, pp. 325-336, 2018

[8] P. Nakmuenwai, F. Yamazaki, and W. Liu, "Automated extraction of inundation areas from multi-temporal dual-polarization RADARSAT-2 images of the 2011 Central Thailand Flood," Remote Sensing, Vol.9, Issue 1, No.78, doi: 10.3390/rs9010078, 2017.

[9] W. Liu and F. Yamazaki, "Detection of inundation areas due to the 2015 Kanto and Tohoku torrential rain in Japan based on multi-temporal ALOS-2 imagery," Natural Hazards and Earth System Sciences, Vol.18, pp. 1905-1918, doi: 10.5194/nhess-18-1905-2018, 2018.

[10] L. Pulvirenti, N. Pierdicca, M. Chini, and L. Guerriero, "An algorithm for operational flood mapping from Synthetic Aperture Radar (SAR) data using fuzzy logic," Natural Hazards and Earth System Sciences, Vol.11, pp. 529-540, doi: 10.5194/nhess-11-529-2011, 2011.

[11] L. Giustarini, R. Hostache, P. Matgen, G. J. P. Schumann, P. D. Bates, and D. C. Mason, "A change detection approach to flood mapping in urban areas using TerraSAR-X," IEEE Trans. on Geoscience and Remote Sensing, Vol.51, pp. 2417-2430, doi: 10.1109/TGRS.2012.2210901, 2013.

[12] D. C. Mason, R. Speck, B. Devereux, G. J.-P. Schumann, J. C. Neal, and P. D. Bates, "Flood detection in urban areas using TerraSAR-X," IEEE Trans. on Geoscience and Remote Sensing, Vol.48, pp. 882-894, doi: 10.1109/TGRS.2009.2029236, 2009.

[13] D. C. Mason, I. J. Davenport, C. N. Neal, Schumann, G. J.-P. Schumann, and P. D. Bates, "Near real-time flood detection in urban and rural areas using high-resolution synthetic aperture radar images," IEEE Trans. on Geoscience and Remote Sensing, Vol.50, pp. 3041-3052, doi: 10.1109/TGRS.2011.2178030, 2012.

[14] G. Nico, M. Pappalepore, G. Pasquarie, A. Refice, and S. Smare, "Comparison of SAR amplitude vs. coherence flood detection method – A GIS application," Int. J. of Remote Sensing, Vol.21, pp. 1619-1631, doi: 10.1080/014311600209931, 2000.

[15] M. Chini, L. Pulvirenti, and N. Pierdicca, "Analysis and interpretation of the COSMO-SkyMed observation of the 2011 Tsunami," IEEE Trans. on Geoscience and Remote Sensing, Vol.9, pp. 467-571, doi: 10.1109/LGRS.2011.2182495, 2012.

[16] L. Pulvirenti, M. Chini, N. Pierdicca, and G. Boni, "Use of SAR data for detecting floodwater in urban and agricultural areas: the role of the interferometric coherence," IEEE Trans. on Geoscience and Remote Sensing, Vol.54, pp. 1532-1544, doi: 10.1109/TGRS.2015.2482001, 2016.

[17] A. B. Rimba and F. Miura, "Evaluating the extraction approaches of flood extended area by using ALOS-2/PALSAR-2 images as a rapid response to flood disaster," J. of Geoscience and Environment Protection, Vol.5, pp. 40-61, doi: 10.4236/gep.2017.51003, 2017.

[18] Y. Kwak, S. H. Yun, and Y. Iwami, "A new approach for rapid urban flood mapping using ALOS-2/PALSAR-2 in 2015 Kinu river flood, Japan," Proc. 2017 IEEE Int. Geoscience and Remote Sensing Symp., pp. 1880-1883, doi: 10.1109/IGARSS.2017.8127344, 2017.

[19] Japan Meteorological Agency (JMA), "Weather bulletins of Okayama Prefecture on July 10, 2018," 2018, https://www.jma-net.go.jp/okayama/topix/20180710.pdf (in Japanese) [accessed November 6, 2018]

[20] Okayama Prefectural Government, "About damage conditions until August 23, 2018 due to the July 2018 Western Japan torrential rain," 2018, http://www.pref.okayama.jp/uploaded/life/574060_4675221_misc.pdf (in Japanese) [accessed November 6, 2018]

[21] Geospatial Information Authority of Japan (GSI), "Digital country map web," 2018, https://maps.gsi.go.jp/ (in Japanese) [accessed November 6, 2018]

[22] Geospatial Information Authority of Japan (GSI), "Base map information," http://fgd.gsi.go.jp/download/menu.php (in Japanese) [accessed November 6, 2018]

[23] Japan Aerospace Exploration Agency (JAXA), "ALOS Research and Application Project of EORC," 2017, https://www.eorc.jaxa.jp/ALOS-2/en/calval/calval_index.htm [accessed November 6, 2018]

[24] S. Hashimoto, T. Tadono, M. Onosata, M. Hori, and K. Shiomi, "A new method to derive precise land-use and land-cover maps using multi-temporal optical data," J. of The Remote Sensing Society of Japan, Vol.34, No.2, pp. 102-112, doi: 10.11440/rssj.34.102, 2014 (in Japanese).

[25] Japan Aerospace Exploration Agency (JAXA), "High-resolution land-use and land-cover maps," 2016, http://www.eorc.jaxa.jp/ALOS/lulc/jlulc_jpn.htm (in Japanese) [accessed November 6, 2018]

[26] D. M. W. Powers, "Evaluation: from precision, recall and F-measure to ROC, informedness, markedness & correlation," J. of Machine Learning Technologies, Vol.2, No.1, pp. 37-63, 2011.

[27] K. Ouchi, N. Ishitsuka, and H. Wang, "On the Bragg Scattering observed in L-Band synthetic aperture radar images of flooded rice fields," IEICE Trans. on Communications, Vol.89-B, No.8, pp. 2218-2225, doi: 10.1093/ietcom/e89-b.8.2218, 2006.

[28] Weathernews Inc., "Indundation conditions in the maximum of flood depths," 2018, https://weathernews.jp/s/gensai/rain_enq201807/map.html (in Japanese) [accessed November 6, 2018]

[29] Geospatial Information Authority of Japan (GSI), "Information for the July 2018 Western Japan torrential rain," 2018, http://www.gsi.go.jp/BOUSAI/H30.taihuu7gou.html (in Japanese) [accessed November 6, 2018]

Name:
Wen Liu

Affiliation:
Assistant Professor, Graduate School of Engineering, Chiba University

Address:
1-33 Yayoi-cho, Inage-ku, Chiba 263-8522, Japan

Brief Career:
2010-2013 Ph.D. of Engineering, Chiba University
2013-2014 JSPS Postdoctoral Fellowship for Foreign Researchers, Tokyo Institute of Technology
2014- Assistant Professor, Graduate School of Engineering, Chiba University

Selected Publications:
• "Estimation of three-dimensional crustal movements in the 2011 Tohoku-oki, Japan earthquake from TerraSAR-X intensity images," Natural Hazards and Earth System Sciences, Vol.15, pp. 637-645, 2015.
• "Extraction of Tsunami Flooded Areas and Damaged Buildings in the 2011 Tohoku, Japan Earthquake from TerraSAR-X Intensity Images," Earthquake Spectra, ERRI, Vol.29, No.S1, pp. S183-2000, 2013.

Academic Societies & Scientific Organizations:
• Japan Society of Civil Engineers (JSCE)
• Remote Sensing Society of Japan (RSSJ)
• Institute of Electrical and Electronics Engineers (IEEE)

Name:
Fumio Yamazaki

Affiliation:
Professor, Graduate School of Engineering, Chiba University

Address:
1-33 Yayoi-cho, Inage-ku, Chiba 263-8522, Japan

Brief Career:
1978- Research Engineer, Shimizu Corporation
1989- Associate Professor, Institute of Industrial Science, The University of Tokyo
2001- Professor, Asian Institute of Technology (AIT)
2003- Professor, Department of Urban Environment Systems, Chiba University

Selected Publications:
• W. Liu and F. Yamazaki, "Detection of Crustal Movement from TerraSAR-X intensity images for the 2011 Tohoku, Japan Earthquake," Geoscience and Remote Sensing Letters, Vol.10, No.1, pp. 199-203, 2013.
• A. Meslem, F. Yamazaki, and Y. Maruyama, "Accurate evaluation of building damage in the 2003 Boumerdes, Algeria earthquake from QuickBird satellite images," J. of Earthquake and Tsunami, Vol.5, No.1, pp. 1-18, 2011.

Academic Societies & Scientific Organizations:
• Japan Society of Civil Engineers (JSCE)
• American Society of Civil Engineering (ASCE)
• Seismological Society of America (SSA)
• Earthquake Engineering Research Institute, USA (EERI)

Name:
Yoshihisa Maruyama

Affiliation:
Associate Professor, Graduate School of Engineering, Chiba University

Address:
1-33 Yayoi-cho, Inage-ku, Chiba 263-8522, Japan

Brief Career:
2004 Completed Doctor Course of Graduate School, Department of Civil Engineering, The University of Tokyo
2004-2005 Postdoctoral Research Fellow, Center for Urban Earthquake Engineering, Tokyo Institute of Technology
2005-2009 Assistant Professor, Department of Urban Environment Systems, Chiba University
2009- Associate Professor, Department of Urban Environment Systems, Chiba University

Selected Publications:
• Y. Maruyama and M. Sakemoto, "Development of nationwide amplification map of response spectrum for Japan based on station correction factors," Earthquakes and Structures, Vol.13, No.1, pp. 17-27, 2017.
• Y. Maruyama, S. Nagata, and K. Wakamatsu, "Damage assessment of water distribution pipelines after the 2011 off the Pacific Coast of Tohoku Earthquake," J. of Energy Challenges and Mechanics, Vol.2, No.4, pp. 144-149, 2015.

Academic Societies & Scientific Organizations:
• Japan Society of Civil Engineers (JSCE)
• Japan Association for Earthquake Engineering (JAEE)
• Institute of Social Safety Science (ISSS)